Numerical simulations of cone penetration tests in cemented sandstone

Aigerim Rakhimzhanova[a,*], Colin Thornton[b], Yerlan Amanbek[a], Yong Zhao[a]

[a] *Nazarbayev University, Nur-Sultan, Kazakhstan, 010000*
[b] *University of Birmingham, Edgbaston, Birmingham B15 2TT, UK*

Abstract

In this study, three-dimensional simulations of cone penetration tests (CPT) in cemented sandstone have been carried out using the Discrete Element Method (DEM). The particle size distribution of the sandstone analogue samples from the Ustyurt-Buzachi Sedimentary Basin was replicated with the numerical samples. Numbers of numerical CPT tests at different bond strength values were performed with the penetrometer vertically moved down at a constant rate. The results of the real-world particle size distribution show that the cone penetration resistance and sleeve friction increase with increasing depths; and with increase in bond strength the cone resistance and side friction decrease, while the friction ratio increases. The result of numerical CPT tests in cemented sandstone was found to be in good agreement with the Soil Behaviour Type (SBT) classification system from CPT data.

Keywords:
Discrete Element Method; cone penetration; cemented sandstone

1. Introduction

The main applications of the cone penetration test (CPT) in geotechnical engineering are for classification and identification of soil types, and for stratigraphic profiling. In a field cone penetration test, a cone with its sleeve is pushed down into the ground at a constant rate, where the cone resistance

*Corresponding authors
Email address: aigerim.rakhimzhanova@nu.edu.kz (Aigerim Rakhimzhanova)

determined by the force required pushing the tip of the cone and the sleeve friction is determined by the force required to push the sleeve through the soil. Then the friction ratio is calculated by the ratio between sleeve friction and cone resistance (measured as a percentage). The classification of soil type can be identified from such basic CPT data.

Here, we provide a brief summary of the literature relating to the cone penetration test in granular soils that has been numerically studied using the Discrete Element Method (DEM) proposed by Cundall and Strack (1979). Huang and Ma (1994) and Jiang et al. (2006) numerically (2D) studied the mechanism of deep penetration in granular soils; Jiang et al. (2014) numerically (2D) examined the mechanism of inclined CPT tests in granular ground; Jiang et al. (2015) numerically (2D) studied the CPT mechanism under different gravity conditions; Arroyo et al. (2011), Ciantia et al. (2016) and Butlanska et al. (2010, 2013) numerically (3D) modelled the CPT test in a calibration chamber taking into account the particle crushing behaviour.

The paper presents results obtained from 3D DEM simulations of cone penetration tests on medium dense samples of cemented sandstone. This research extends recent development of a simple 3D bond contact model for cemented sandstone material in Rakhimzhanova et al. (2019, in press). This study was successfully applied to the triaxial compression tests of cemented sandstone, where the stress-strain responses of the numerical samples were found to be in good agreement with the experimental results of cemented sandstone.

This paper is divided into four parts. In Section 2, the numerical contact model will be described. The numerical simulation of cone penetration test details and procedure are described in Section 3. The numerical results are presented in Section 4 and conclusions are reported in Section 5.

2. Numerical methods

2.1. The Discrete Element Method

In the theoretical model integrated in the DEM model, all motions of particles are guided by Newton's equations of motion and the components ($i = 1, 2, 3$) in x-, y-, and z- directions of the translational and rotational accelerations of each particle are given by Eq.(1) and Eq.(2), respectively:

$$m_i \frac{dv_i}{dt} = F_{ci} + m_i g_i \tag{1}$$

$$I \frac{dw_i}{dt} = F_{ti} R \tag{2}$$

where, m_i, v_i and ω_i are the mass, linear and angular velocities of particle i, respectively; g is the gravity, F_{ci} is the solid interaction force between particles, $F_{ti}R$ are the moments due to the tangential components of the contact forces, and I is the moment of inertia.

2.2. Contact models

2.2.1. No adhesion

In all simulations, particles are considered to be elastic and frictional, where the particle-particle and wall-particle contact forces without adhesion are calculated using the theories of Hertz Hertz (1881) to determine the normal force, and Mindlin (1949) Mindlin (1949) to calculate the tangential force. According to the Hertz theory, the normal force F_n due to relative approach α of the spheres is

$$F_n = \frac{4}{3} E^* \sqrt{R^* \alpha^3} \tag{3}$$

where, $1/R^*$ the relative curvature of the surface of contacting spheres of radii R_i $(i = 1, 2)$ and is defined as

$$\frac{1}{R^*} = \frac{1}{R_1} + \frac{1}{R_2} \tag{4}$$

and E_i and ν_i $(i = 1, 2)$ are the Young's moduli and Poisson ratios for the two elastic spheres, respectively and the relative Young's modulus is given below

$$\frac{1}{E^*} = \frac{(1 - \nu_1^2)}{E_1} + \frac{(1 - \nu_2^2)}{E_2} \tag{5}$$

From Eq.(3) the normal contact stiffness is defined as

$$k_n = 2E^* \sqrt{R^* \alpha} \tag{6}$$

The tangential force depends on the normal force (increasing or decreasing) and it is calculated incrementally. For the increasing normal force $F_n \geq 0$, the tangential force at the time step i^{th} is

$$F_t^i = F_t^{i-1} + k_t^i \Delta \delta \tag{7}$$

and for the decreasing normal force $F_n < 0$, it is defined as

$$F_t^i = F_t^{i-1}\left(\frac{k_t^i}{k_t^{i-1}}\right) + k_t^i \Delta\delta \tag{8}$$

where δ is the rigid displacement of the sphere centers. For $F_n \geq \mu F_n$, the tangential force is given as

$$F_n = \mu F_n \tag{9}$$

where μ is the friction coefficient. The tangential contact stiffness is calculated by

$$k_t = 8G^* \sqrt{R^* \alpha} \tag{10}$$

and it is prescribed by the 'no-slip' solution of Mindlin (1949), where G^* is the complex shear modulus defined by

$$\frac{1}{G^*} = \frac{(2-\nu_1)}{G_1} + \frac{(2-\nu_2)}{G_2} \tag{11}$$

2.2.2. With adhesion

A simple 3D bond contact model for cemented sandstone material developed by Rakhimzhanova et al. (2019, in press) was used to calculate the interparticle normal contact force with adhesion, which simply modified the existing JKR model for auto-adhesive silt sized particles provided by Johnson et al. (1971), and the Mindlin (1949) no-slip model to calculate the tangential contact force. Johnson (1977)provided the relationship between the normal contact force, F_n, and the relative approach, α (see Fig. 1).

Initially, when two particles come into contact ($\alpha = 0$) due to van der Waals attractive forces, the normal contact force, F_n, instantly drops down to point A and at this point the normal contact force equals $F_n = -8F_{nc}/9$. In case of loading (compression) the normal contact force increases from point A to point B. During the unloading (decompression) the force returns from point B to point A due to the elastic response and the relative approach is equal to 0 (there is still a finite area of contact) and all the work done during the compression will be recovered. The tensile force increases during the extra work from point A to pint C and then decreases until contact between the particles breaks at point D, when $F_n = -5F_{nc}/9$ and the negative relative approach $\alpha = -\alpha_f$, where

$$\alpha_f = \left(\frac{3F_{nc}^2}{16R^* E^{*2}}\right)^{1/3} \tag{12}$$

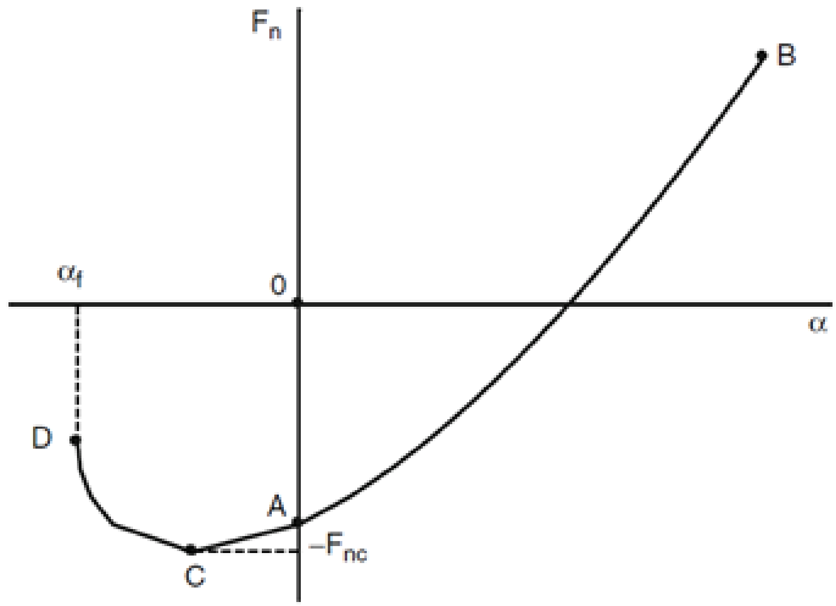

Figure 1: Normal force-displacement curve for JKR theory.

Nevertheless, the rock from the oil field reservoir is sandstone i.e. sand with cement bonds and the cement bonds are not as stretchable and break in a brittle manner. Therefore, in the simple 3D contact model for cemented sandstone material developed by Rakhimzhanova et al. (2019, in press) the bond breaks at point C, where the normal contact force $F_n = -F_{nc}$ and the relative approach $\alpha = -\alpha_f/3^{2/3}$. The maximum tensile force required to break the contact (at point C) is

$$F_{nc} = 1.5\pi\Gamma R^* \tag{13}$$

where Γ is the work of adhesion and $\Gamma = \gamma_1 + \gamma_2 = 2\gamma$ are the surface energies of the two solids. In the simple 3D contact bond model, any subsequent new contact force is calculated by the Hertzian theory.

3. Numerical simulations

In this study, the cone penetration tests were divided into four stages: particle generation, pluvial deposition, compression, cone penetration (see Fig. 3). Three-dimensional DEM simulations of cone penetration tests have been performed using 10000 frictional elastic spheres bonded together over a range of bond strengths (interface energy of adhesion) of $\Gamma = 0, 5, 10, 20$ J/m2 (where $\Gamma = 0$ J/m2 is an uncemented sample) and compressed at 1 MPa of overburden pressure, where in all cases particle rotations were prevented.

3.1. Particle generation and deposition

Eight different particle sizes from the particle size distribution (PSD) data of the cemented analogue samples from the Ustyurt-Buzachi Sedimentary Basin (Fig. 2) measured by Qicpic dynamics image analyzer (Shabdirova et al. (2016)) were randomly generated (Fig. 3a) as a granular gas within a thin rectangular parallelepiped of dimension 8.4 mm in width, 21 mm in height and 1.4 mm in thickness: 0.15 mm (1179), 0.18 mm (1750), 0.2 mm (1505), 0.22 mm (1558), 0.25 mm (1973), 0.275 mm (1119), 0.3 mm (610), 0.355 mm (306). Based on the Unified Soil Classification System (USCS)

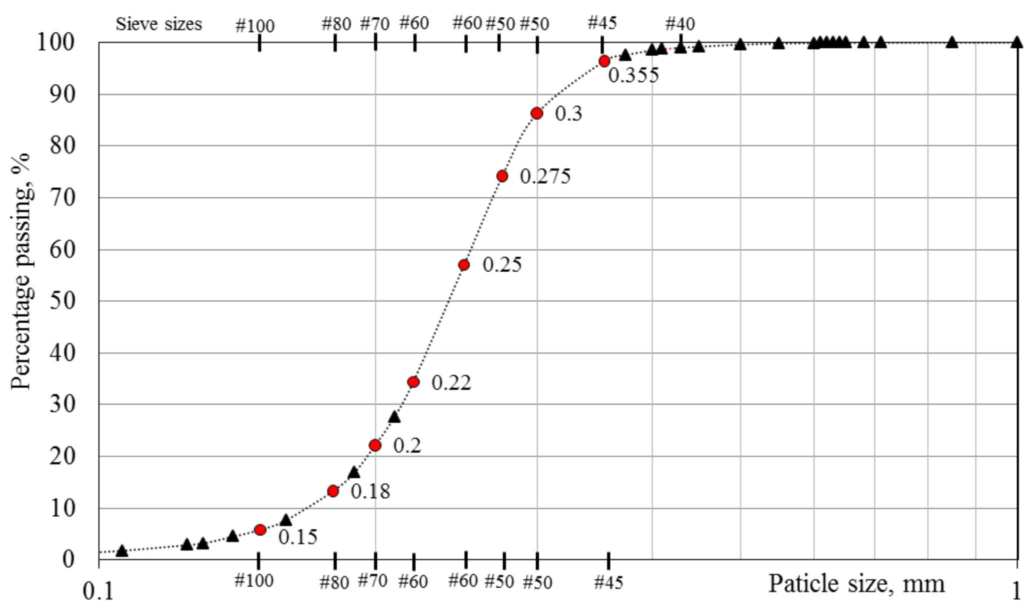

Figure 2: Particle Size Distribution of the reservoir sand from the Ustyurt-Buzachi Sedimentary Basin.

these grain sizes pass through the sieve sizes # 45-100, which indicates that the soil type is S – sand with the subdivision of fine sand. The thin parallelepiped workspace was divided into 720 small DEM boxes (box dimension of 0.0007 mm): 12 boxes in width, 30 in height and 2 in thickness. The following material properties were used for all sand particles: Young's modulus $E = 70$ GPa, Poisson ratio $\nu = 0.3$ and experimental particle density $\rho = 2605$ kg/m3. Further, a vertical gravity field was applied to the system and all particles were pluvially deposited to form the initial homogeneous bed (Fig. 3b). One finite wall was created at the bottom of workspace in order to avoid/prevent the periodic boundary condition at this side. The following material properties of iron were used for all walls: Young's modulus $E = 210$ GPa, Poisson ratio $\nu = 0.29$ and density $\rho = 7900$ kg/m3.

3.2. Compression and cone penetration

Three top finite walls were created at the top of the deposited specimen and moved down at a wall velocity of 0.1 m/s in order to vertically compress the sample (Fig. 3c). When a vertical stress level (overburden pressure) reached 500 kPa, then the bond strength values $\Gamma = 0, 5, 10, 20$ J/m2 were set. When the overburden pressure reached 1 MPa, the top three wall velocities were reset to 0. After the compression of DEM cemented sandstone, a standard cone penetrometer was first created above the bed and then pushed down at a high constant rate of 0.1 m/s in order to avoid computational cost. The penetrometer had a "radius" R of 0.7 mm and an apex angle of 60° (Fig. 3d). It was defined as 2 rigid frictional walls inclined to X-axis at 60° to simulate the cone/tip penetrometer and two rigid vertical frictional walls to simulate the penetrometer sleeve (Fig. 4. During the simulations the cone was always in contact with about 33-35 particles, which provide the resistance value. The initial ground surface is considered as the origin and the distance between the tip point (lowest point of tip) and the origin is defined as the penetration depth y. The cone penetrometer was removed from the penetrated specimen once the cone tip had reached 2/3 of the depth.

4. Numerical results

Figs. 5 a, 5 b and 5 c show the evolution of cone resistance, friction sleeve and friction ratio data at different penetration depths for $\Gamma = 0, 5, 10, 20$ J/m2, respectively. The cone resistance is defined as the vertical pressure measured on the cone

$$q_c = \frac{\sum f_y}{2Rt} \tag{14}$$

where f_y is the vertical contact force acting on inclined wall (cone); R is the cone radius; t is the thickness of the bed ($t = 2R$), and the frictional sleeve,

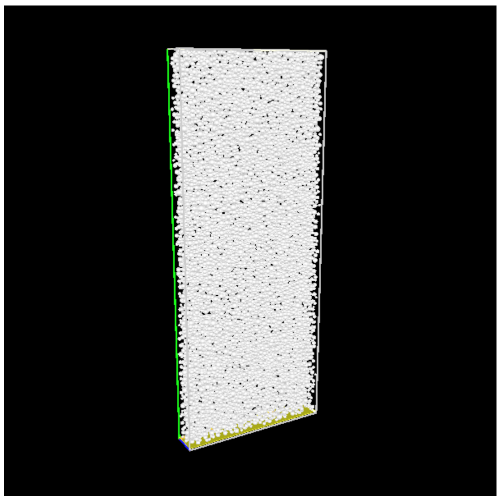

(a) Particle generation

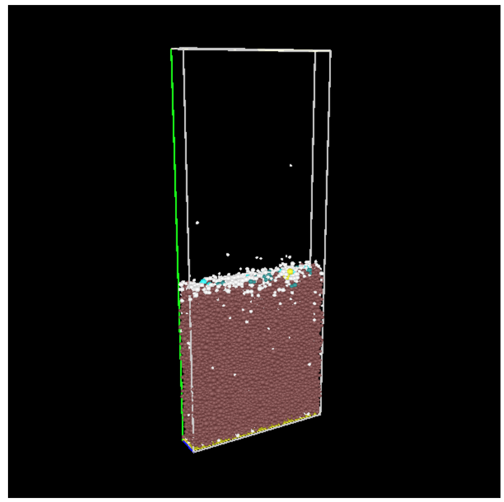

(b) Pluvial deposition

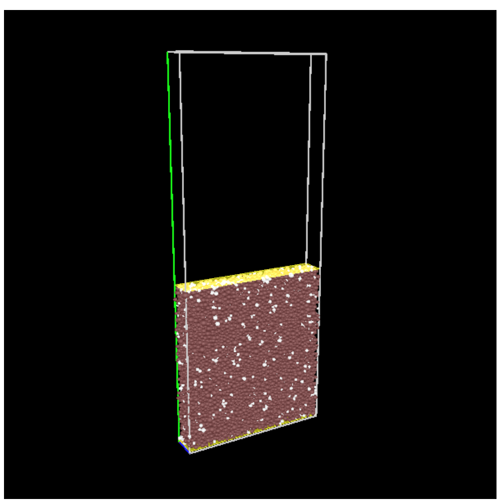

(c) Compression

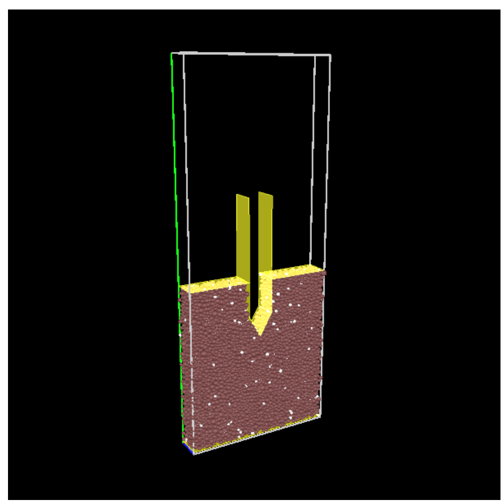

(d) Cone perforation

Figure 3: 3D DEM cone penetration simulation stages.

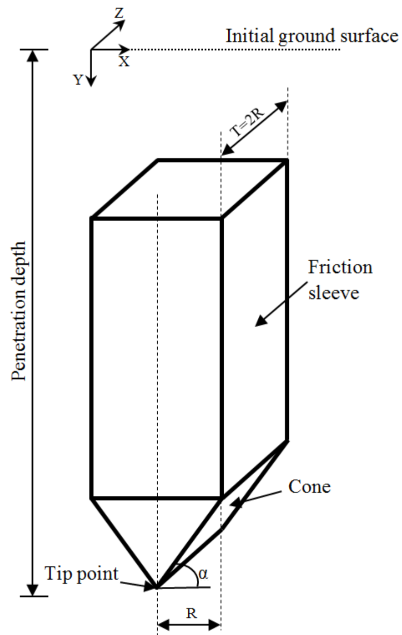

Figure 4: Cone penetrometer (modified from Jiang et al. (2006).

f_c, is defined as

$$f_s = \frac{\sum f_y}{2Ht} \tag{15}$$

where f_y is the vertical contact force acting on the frictional sleeve; H is the frictional sleeve height in the ground.

It can be seen that the cone penetration resistance and sleeve friction increase with increasing depths. Similar behavior was obtained in 2D DEM CPT simulations reported by Jiang et al. (2006), and in the real field CPT data reported by Robertson (1990). The friction ratio, R_f, is calculates as

$$R_f = \frac{f_c}{q_c} 100\% \tag{16}$$

where q_c is from Eq.(14) and f_s from Eq.(15). The results show that with increase in bond strength the cone resistance and side friction decrease, but the friction ratio increases. Robertson et al. (1986) and Robertson (1990) proposed CPT-based charts as a guide to predict the Soil Behavior Type (SBT) based on the basic field CPT data where only the total cone penetration

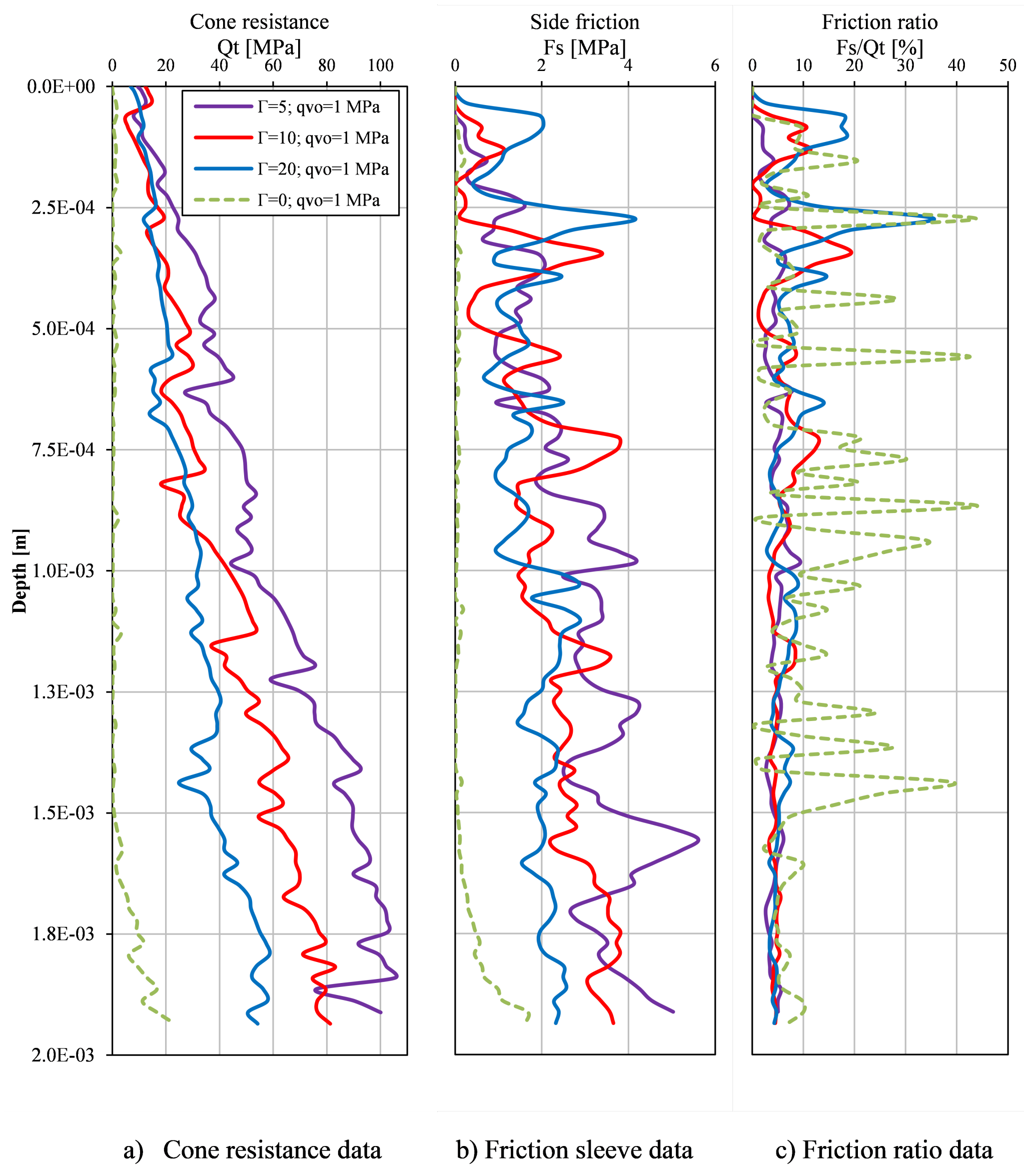

Figure 5: The numerical CPT data.

resistance, q_t, and the sleeve friction, f_c, are available (Fig. 6). Campanella and Robertson (1982) proposed that the cone resistance, q_c, can be corrected to the total cone resistance, q_t, as

$$q_t = q_c + u(1 - a) \tag{17}$$

where u is the pore pressure measured between the cone tip and the friction sleeve and a is the net area ratio calculated as $a = d^2/D^2$, where d is the diameter of the friction sleeve and D is the diameter of the cone. This correction should be made to account for unequal end area effects because the water pressure acts on an area immediately behind the cone tip. Since the numerical simulations of cone penetration tests conducted on dry particles the net area, a, was equal to 1 and the assumption of $q_c = q_t$ has been made.

The data points of 3D DEM simulations of CPT of cemented sandstone have been added in this classical soil classification chart. The average values of cone resistance and friction sleeve was taken starting from the depth 0.0015 m, once they became more stable. It is shown that the CPT data of samples with higher bond strengths of Γ = 10 and 20 J/m2 locates in SBT zone 12, which is identified as overconsolidated or cemented sand to clayey sand; and Γ = 0 and 5 J/m2 locate in SBT zone 11, which behaves as very stiff, overconsolidated fine grained sand.

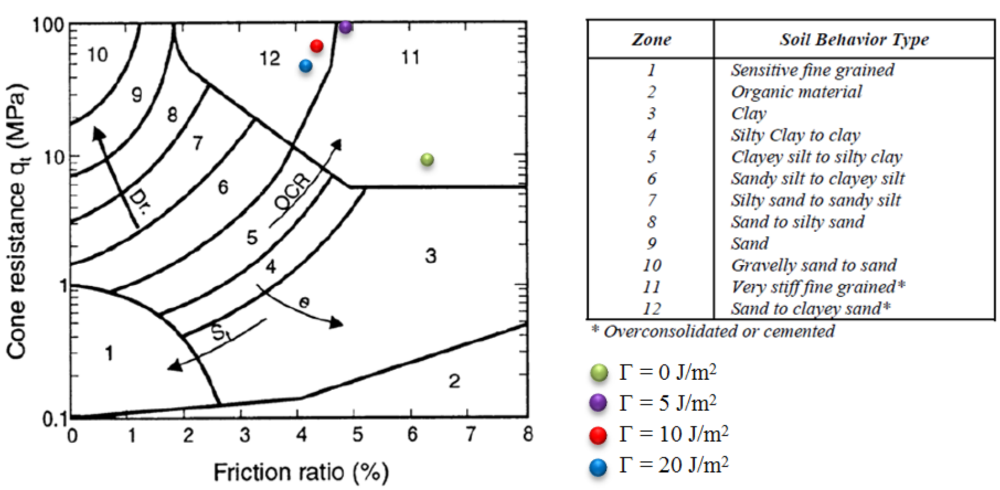

Figure 6: CPT soil behavior type chart, as proposed by Robertson et al. (1986).

The SBT zone 11 and 12 for all samples can be explained as at the end of compression stage, the material that contains only fine sand particles

(Fig. 2) had a porosity of about 0.38, which are similar to those porosities obtained for 3D DEM simulations of triaxial compression tests of cemented sandstone on medium dense samples compressed at 1MPa and $\Gamma = 0, 5, 10, 20$ J/m (Rakhimzhanova et al. (2019, in press)). For $\Gamma = 5$ J/m2 it can be explained that, at the lowest value of $\Gamma = 5$ J/m2, the bond strength is soft and more bonds were broken, compared with higher values of $\Gamma = 10$ and 20 J/m2, with a tendency to behave like an uncemented sand. The SBT zone 11 for uncemented sand ($\Gamma = 0$ J/m2) can be explained in that the sand becomes stiffer as initial density and/or confining pressure increases (frictional response). Similar behavior has been experimentally obtained for compressive behavior of fine sand by Kabir et al. (2010) and numerically captured by Rakhimzhanova et al. (2019, in press).

5. Conclusion

In this paper, the 3D DEM simulations of cone penetration test of cemented sandstone have been investigated at different values of bond strength. Material properties of reservoir analogue sandstone samples from the Ustyurt-Buzachi Sedimentary Basin were replicated for the numerical samples. A simple 3D bond contact model developed for cemented sandstone material and the identified bond strength values to be used for comparison with experimental results by Rakhimzhanova et al. (2019, in press) were used for the simulations of CPT test. The results show that with increase in bond strength the cone resistance and side friction decrease, while the friction ratio increase; the cone resistance and side friction increase with increase in penetration depths.

It has been demonstrated that the numerical CPT tests result of cemented sandstone are in good agreement with the Soil Behavior Type (SBT) classification system from CPT data. The findings suggest that this method could also be useful for practicing engineers to control perforation technique in the sandstone field.

Acknowledgements

This research was supported by the EU Project GEO-RAMP (H2020-MSCA-RISE-2014 GA 645665) and by the Nazarbayev University Faculty Development Competitive Research Grant No 110119FD4502. The authors gratefully acknowledge Prof. Stefano Utili (Newcastle University) and Dr.

Helen Cheng (University College London) for their help during the first author's visits to the UK.

References

Arroyo, M., Butlanska, J., Gens, A., Calvetti, F., Jamiolkowski, M., 2011. Cone penetration tests in a virtual calibration chamber. Géotechnique 61, 525–531.

Butlanska, J., Arroyo, M., Gens, A., 2010. Virtual calibration chamber cpt on ticino sand, in: 2nd International Symposium on Cone Penetration Testing, Huntington Beach, CA, USA.

Butlanska, J., Arroyo, M., Gens, A., O'Sullivan, C., 2013. Multi-scale analysis of cone penetration test (cpt) in a virtual calibration chamber. Canadian geotechnical journal 51, 51–66.

Campanella, R., Robertson, P., 1982. State-of-the-art in in-situ testing of soils; developments since 1978, engineering, in: Foundation Conference on Updating Subsurface Sampling of Soils and Rocks and Their In-Situ Testing, p. 23.

Ciantia, M.O., Arroyo, M., Butlanska, J., Gens, A., 2016. Dem modelling of cone penetration tests in a double-porosity crushable granular material. Computers and Geotechnics 73, 109–127.

Cundall, P.A., Strack, O.D., 1979. A discrete numerical model for granular assemblies. geotechnique 29, 47–65.

Hertz, H., . Über die berührung fester elastischer körper. journal für die reine und angewandte mathematik 92 (1881), s. 156–171. .

Huang, A.B., Ma, M.Y., 1994. An analytical study of cone penetration tests in granular material. Canadian Geotechnical Journal 31, 91–103.

Jiang, M., Dai, Y., Cui, L., Shen, Z., Wang, X., 2014. Investigating mechanism of inclined cpt in granular ground using dem. Granular Matter 16, 785–796.

Jiang, M., Liu, F., Wang, H., Wang, X., 2015. Investigation of the effect of different gravity conditions on penetration mechanisms by the distinct element method. Engineering Computations 32, 2067–2099.

Jiang, M., Yu, H.S., Harris, D., 2006. Discrete element modelling of deep penetration in granular soils. International Journal for Numerical and Analytical Methods in Geomechanics 30, 335–361.

Johnson, K., 1977. Adhesion at the contact of solids. Theoretical and applied mechanics , 133–143.

Johnson, K.L., Kendall, K., Roberts, A., 1971. Surface energy and the contact of elastic solids. Proceedings of the royal society of London. A. mathematical and physical sciences 324, 301–313.

Kabir, M.E., Song, B., Martin, B.E., Chen, W., 2010. Compressive behavior of fine sand. Sandia National Laboratories, New Mexico .

Mindlin, R., 1949. Compliance of elastic bodies in contact. J. Appl. Mech., ASME 16, 259–268.

Rakhimzhanova, A.K., Khamitov, F.A., Minh, N.H., Thornton, C., in press. 3d dem simulations of triaxial compression tests of cemented sandstone., in: Proceedings of IS Atlanta 2018 Symposium on Geomechanics from Micro to Macro in Research and Practice, Atlanta, USA.

Rakhimzhanova, A.K., Thornton, C., Minh, N.H., Fok, S.C., Zhao, Y., 2019. Numerical simulations of triaxial compression tests of cemented sandstone. Computers and Geotechnics 113, 103068.

Robertson, P., 1990. Soil classification using the cone penetration test. Canadian Geotechnical Journal 27, 151–158.

Robertson, P.K., Campanella, R., Gillespie, D., Greig, J., 1986. Use of piezometer cone data, in: Use of in situ tests in geotechnical engineering, ASCE. pp. 1263–1280.

Shabdirova, A., Bissekenova, Z., Minh, N., Kim, J., et al., 2016. Sample preparation method of clay-rich sandstone analogue of sandstone reservoirs in kazakhstan, in: 50th US Rock Mechanics/Geomechanics Symposium, American Rock Mechanics Association.